

A Geometrical Approach for the Automatic Detection of Liquid Surfaces in 3D Computed Tomography Baggage Imagery

Lounis Chermak*, Toby P. Breckon**, Greg T. Flitton*, Najla Megherbi*

*School of Engineering, Cranfield University, Cranfield, UK

**School of Engineering & Computing Sciences, Durham University, Durham, UK

Abstract—This study presents a novel method for liquid detection within 3D Computed Tomography (CT) baggage inspection imagery. Liquid detection within airport security is currently of significant interest due to security threats associated with liquid explosives. In this paper we propose a robust technique based on the automatic identification of universal geometric properties of liquids within 3D space. The proposed approach is based on two stages of geometric fitting. Firstly, we identify the 3D plane which fits to the horizontally oriented surface of the liquid recognizing the universal self-leveling property of liquids in any given container. Secondly we conduct 2D shape analysis to highlight the shape of the liquid surface at a given level within the container using a least squares elliptical fitting approach. The proposed approach relies on the fact that occurrences of such perfectly aligned horizontal planes within a 3D CT security baggage scan are generally unlikely. Occurrences of such instance are thus indicative of liquid presence. Our results, over an extended set of complex test examples, confirm a liquid detection rate of 85%-98% with a moderate processing time. Furthermore as this proposed approach is based purely on the geometric properties of liquids and robust geometrical shape detection, this methodology is intrinsic to the 3D nature of the resulting CT data and not dependent on any exemplar training imagery.

Index Terms—Computed Tomography; Aviation Security; 3D Security Screening; Baggage Imagery; Planar Fitting; Elliptical Fitting; liquid detection

I. INTRODUCTION

The motivation behind this work emanates from the requirement to detect the presence of liquids within transport security screening processes. Specifically this work consists of investigating and developing a methodology for the automatic detection of liquids items within 3D Computed Tomography (CT) imagery. Recently the use of 3D CT imagery, akin to that in medicine, has received increasing attention as a security screening aspect within transport security screening [1], [2]. Indeed the development of high-speed 3D CT baggage scanners allows the unique physical and 3D geometrical properties of baggage and parcel items to be captured in an efficient way [3].

The principle of 3D CT scanners lies in X-ray imaging which consists in measuring the absorption of the X-ray beam attenuation of objects within the scanner. As an extension of classical 2D X-ray security scanner the baggage item is scanned as a sequence of 2D X-ray slices [4], [5]. These slices are used as an image stack to create a 3D CT volume [5]. As a consequence the scanned 3D object is captured according to

the density of its material component at every 3D location (i.e. CT voxel location). This additionally allows 3D visualization of objects within a complex 3D baggage scan based on their density information (Figure 1a). By contrast, conventional 2D X-ray security imagery can be somewhat more difficult to process (both manually and automatically) due to the inherent problem of object inter-occlusion within the planar 2D image projection of the real-world 3D baggage/parcel (e.g. Figure 1b) [3].

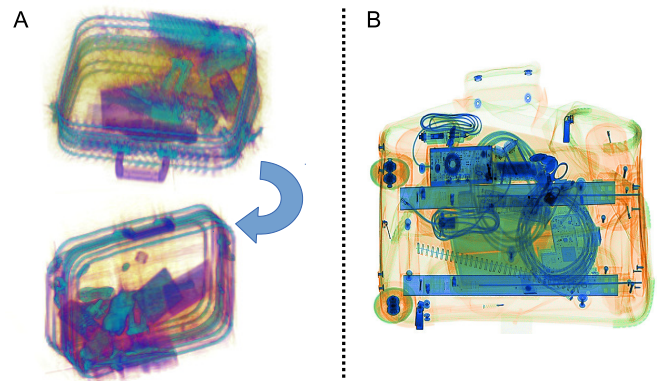


Figure 1. Exemplar 3D CT image (A) and exemplar 2D X-ray image (B)

By contrast, the use of 3D CT imagery overcomes ambiguities caused by such inter-occlusion (within conventional 2D X-ray imagery) and also allows objects to be isolated based on the CT density information recorded at each voxel (in Hounsfield units (HU) that measure radiodensity [5]). This enables utilization of both material density information, for which *a priori* knowledge of common materials is well-established [6], and 3D geometric shape detection in voxel-space for the automated detection and classification of objects within the CT scan imagery [7], [8], [9], [10], [11]. In this work, we take specific advantage of both the 3D geometric properties of objects within such CT baggage imagery and additionally the physical behavior of liquid within a given 3D container. Overall this concept consists of two main aspects: a) the ability of liquids to “self level” to the ground plane as a consequence of gravity (Figure 2b) the morphological property of liquids to adapt and fill any 3D container space constraints.

This first characteristic is the foundation of the liquid detection methodology we propose. Due to the horizontal

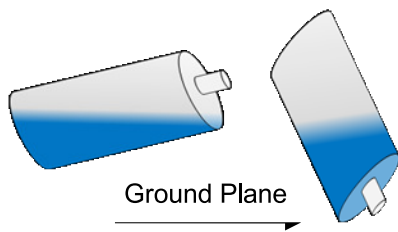


Figure 2. The basic liquid horizontal leveling property

leveling property of liquids, the top surface of a stationary liquid is almost perfectly parallel to the ground plane (and consequently in our case to the orientation of the baggage item within the scanner). This property can be readily detected via geometric planar fitting [12] in 3D voxel-space. By contrast, the occurrence probability for such a perfectly aligned plane within a scanned baggage item, consisting of random objects and clutter, is generally accepted as low (discounting surface water instances on the exterior of the baggage item). As the content of a given baggage/parcel item is likely to be complex and disorientated with respect to the ground plane, liquid containers may be potentially set in any 3D position/orientation within the baggage. In any such occurrence the “self leveling” property (Figure 2) will always hold true for all but the most viscous of liquids.

Our second characteristic concerns itself with the sense that within any given container void, the morphological self filling property of liquids will mean that a liquid signature in the shape of the container will be present within any identified horizontal liquid plane. In addition to the presence of the a perfectly aligned 3D planar surface, this now introduces a second “within the plane” signature - i.e. the presence of a consistent morphologically filled shape within that detected plane. Our use of geometric planar fitting [13] is complemented by geometric elliptical fitting in 2D (i.e “within the plane”) for this task [14].

II. PRIOR WORK

In general, existing techniques targeting the automated detection of (specifically) liquid explosives is varied covering the use of vapor detection, X-ray detection, laser detection, nuclear detection to electromagnetic based approaches [4]. By contrast we concern ourselves with the detection of the presence or absence of liquids in general via automated interpretation of CT baggage imagery.

Current interest in CT imagery within a security screening context stems from their capability in materials-based explosives detection [4], [15]. Dual-Energy Computed Tomography (DECT) [5], whereby objects are scanned at two distinct X-ray energy levels (for each CT slice), provides an effective means for such materials-based discrimination [2]. As a result of this primary explosives detection objective within the aviation-security domain, DECT baggage scanners have become increasingly dominant offering both CT density and materials based information. However, despite overcoming the inherent problem of occlusion within 2D X-ray, demand for high throughput has often meant that 3D CT baggage

imagery typically contains substantial noise, metal-streaking artefacts and voxel resolutions of significantly poorer quality than the modern medical CT equivalent [5], [16] (Figure 1). Prior work has considered denoising and metal artefact reduction in baggage CT imagery [17], [16], [18] although the overall impact on object classification within this space remains unproven [7], [8], [9], [11], [1].

Work on the automated interpretation of CT baggage imagery remains in its infancy [9], [8], [10], [11], [1]. Bi et al. [19] attempted handgun detection within CT baggage imagery. The work did not involve processing the 3D data directly as the problem was reduced to searching for the characteristic cross-section of the handguns and no explicit quantitative or qualitative detection results are presented. Megherbi et al. [9], [10] investigated the detection of bottles, as generalized objects, within CT volumetric data using a normalized histogram of shape index descriptor and rotational invariant 3D Zernike descriptors. Correct classification rates in excess of 98.0% are presented using a relatively small dataset highlighting the data dependency of such machine learning driven approaches. Flitton et al. [8] compare the performance of a 3D visual cortex-based approach to a bag of visual word model using the 3D SIFT descriptor [7], [11], [1]. The cortex-based approach is shown to outperform the bag of visual words approach in the detection of handguns and bottles in manually segmented sub-volumes. Mouton et al. [20] demonstrate a further improvement over the 3D visual cortex model in terms of classification accuracy and processing time using a code-book approach based on extremely randomised clustering forests.

The most similar work to our own [21] proposes a methodology for the detection of planar materials within baggage CT imagery using a 3D extension to the Hough transform. Although carried out within an aviation security context, this work is entirely concentrated on fast detection of 3D planes with a view to improving the quality of scan data within a helical CT scanner (as opposed to liquid detection). The authors propose the detection of basic geometric forms, notably plane detection, to validate the performance and correctness of the CT volume reconstruction algorithms in use within the helical CT scanner machine. Their approach [21] is based on the classical Hough transform applied to 3D CT volumetric imagery for automatic plane detection. The proposed method starts with the use of edge detection within each image slice to identify potential regions of interest upon which Hough line detection is then performed to build up 3D plane detection on a slice-by-slice basis.

By contrast, we propose the joint use of both geometric plane fitting within the, already reconstructed, 3D CT volume itself and secondary confirmation via 2D elliptical fitting within identified planes of interest. This explicitly focuses on a geometric approach for the identification of liquid containers, via their surface properties within 3D CT baggage imagery.

III. METHODOLOGY

Here we propose a liquid detection methodology within 3D CT volumetric baggage imagery based on a two stage approach - primary 3D planar fitting (Section III-B) and

secondary confirmation and localization using 2D elliptical fitting (Section III-C).

A. Pre-processing

From the 3D CT imagery, composed of a dense topology of voxels ($X \times Y \times Z$ topology of CT density samples), we perform two initial stages of pre-processing. This dense dataset is firstly thresholded to produce a sparse set of voxels with CT density corresponding to liquids whereby we use two thresholds at $\tau_{water} \pm \alpha$ ($\alpha = 50$ HU, approximately 5% variation within the Hounsfield scale [5]). All CT scanners are calibrated such that distilled water has a density value of zero, $\tau_{water} = 0$ HU [5]. The resulting threshold range encompasses a range of liquid viscosity ranging from fats (~ -50 HU) to blood and soft tissue ($\sim +30 \rightarrow 45$ HU). This is illustrated in Figure 3, where the bottle containing liquid is clearly distinguishable in the cluttered baggage image from the other items falling within the same CT density range. After thresholding the only compact spatial cluster of voxels remaining is the bottle containing liquid whereas other remaining voxels are sparsely distributed (as noise and are hence largely transparent within the volume rendering of Figure 3). This data refinement significantly reduces the level of background clutter, allowing subsequent 3D planar fitting to focus on the detection of liquid derived surface features.

A secondary pre-processing step, denoted as slice differencing, performs a vertical search through the thresholded volume (Figure 3, right) to determine the maximal density differences between two adjacent voxel slices (with reference to the horizontal plane). This will represent a horizontal slice region where a significant transition from liquid to air is occurring with this volume. Empirically, we use a threshold on these slice-to-slice differences, τ_{slice} , which is set based on the real-world dimensions of the liquid surface we wish to detect. Based on detection within typical consumer liquid containers found within the test baggage items used in this study and a uniform voxel sampling in the horizontal plane of 512×512 at 2.5mm^3 per voxel, we set $\tau_{slice} = 350$ (i.e. a potential liquid to air surface transition is determined by a difference at $\frac{350}{512^2} = 0.1\%$ of surface voxels which translates as a surface area of $350 \times 2.5\text{mm}^2$ (875mm^2) within the slice).

B. 3D Planar Fitting

In our first stage of liquid surface detection, we employ geometric fitting to identify potential planar occurrences near to the horizontal plane. We perform a vertical search through the CT volume image for subsets of the remaining voxels (Figure 3, right) that correspond to a significant planar artifact using an adaptation of the RANdom SAMple and Consensus (RANSAC) 3D planar fitting algorithm of [12] in regions where maximal differences between two adjacent horizontal slices occur (Section III-A, corresponding to the liquid to air transition surface region).

RANSAC is an robust statistical technique for the generalized fitting of a mathematical model to data points based on iterative randomized subset selection and evidential evaluation [22]. From a given data set containing outliers (e.g. (Figure

3, right) a random subset is isolated to form a parameter hypothesis for a given model, upon which a voting scheme (i.e. consensus forming) identifies the most likely parametrization present given the data (*maximum a posteriori*). Using the mathematical model of a 3D plane (Eqn. 1) we employ RANSAC using a sliding window mechanism over a set of s_w horizontal slices within the volume (parallel to the scan bed of the CT scanner, advancing vertically top to bottom - Figure 4). The use of such a sliding window approach facilitates identifications of liquid surfaces that form planes that cross one or more horizontal planes within the CT volume itself. This accounts for any inaccuracy in the level of the CT scanner relative to the true gravitational ground plane to which the liquid surface plane will level itself (Figure 2). In this work we empirically use a vertical sliding window of $s_w = 5$ (Figure 4).

Our fitting approach considers the standard planar equation in 3D space where (x, y, z) are the coordinates of points lying on plane in \mathbb{R}^3 which is characterized by the four coefficients $\{a_p, b_p, c_p, d_p\}$ as follows:

$$a_p x + b_p y + c_p z + d_p = 0 \quad (1)$$

In our formulation the set of coordinates (x, y, z) corresponds to the voxel data points (x_i, y_i, z_i) within the sliding window sub-sampling used for vertical planar search within the volume (Figure 4). Following from [13], we identify a general method to compute and extract a generalized shape fit for a shape defined by a basis set l parameters/coefficients with $l - 1$ points. From Eqn. 1, we can hence define a plane from 3 data points. In general this method is expressed as least square optimization problem such that given M , a $m \times n$ matrix of rank $r \leq \min(m, n)$, and k , a m -dimensional vector we require to find p_p , a n -dimension parameter vector which minimizes the Euclidean distance of the transform $Mp_p - k$ (in our case $m = n = 3$). This gives Eqn. 2 as follows:

$$Mp_p = k \quad (2)$$

In the case of horizontal planar fitting, where a plane defined by a basis set of three data points, $\{(x_i, y_i, z_i), i \in \{0, 1, 2\}\}$, Eqn. 2 expands to give the following formulation:

$$\begin{bmatrix} 1 & y_0 & z_0 \\ 1 & y_1 & z_1 \\ 1 & y_2 & z_2 \end{bmatrix} \begin{bmatrix} d_p \\ b_p \\ c_p \end{bmatrix} = \begin{bmatrix} x_0 \\ x_1 \\ x_2 \end{bmatrix} \quad (3)$$

where M is composed of measured data points (y_i, z_i) and a constant term, normalised to 1 (corresponding to plane constant d_p), k is a vector the coordinates of measured data points x_i (vertical depth within the volume) and p_p is the vector containing the parameters $\{b_p, c_p, d_p\}$ of the plane (from Eqn. 1). Note that we empirically fix parameter a_p of Eqn. 1, $a_p = 1$, due to horizontal constraint. Following from the formulation of Eqn. 3 we derive the following system of equations:

$$\begin{aligned} d_p + b_p y_0 + c_p z_0 &= x_0 \\ d_p + b_p y_1 + c_p z_1 &= x_1 \\ d_p + b_p y_2 + c_p z_2 &= x_2 \end{aligned} \quad (4)$$

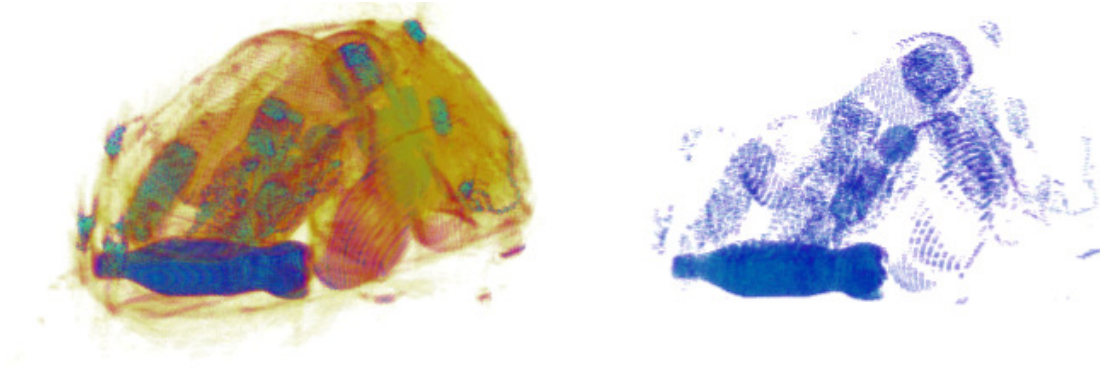


Figure 3. An original 3D CT baggage volume (left) and the same volume after density thresholding, $\tau_{water} \pm \alpha$ (right)

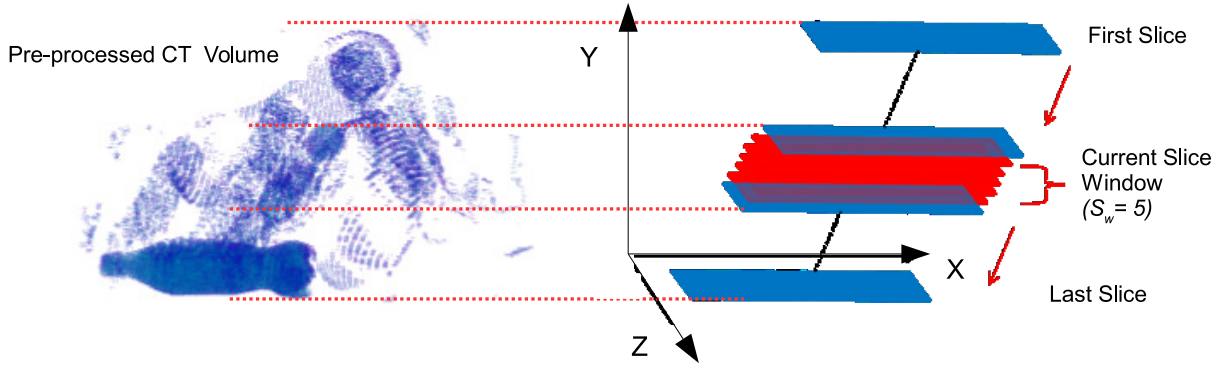


Figure 4. Vertical sliding widow search for planes within the volume

where x is taken as a pivot because in our planar fitting case we desire to fit a plane which is approximately parallel to the $x \leftrightarrow y$ plane and hence perpendicular to the $y \leftrightarrow z$ plane (inside the bounds of the sliding window, i.e. $\pm s_w$ deviation in y). The system shown in Eqn. 4 is resolved by minimization of the error $\| Mp_p - k \| = \epsilon$, derived from Eqn. 2 for an error term, ϵ . Furthermore this can be expanded as follows, to recover p_p , such that:

$$\begin{aligned} \arg \min_{p_p} \| Mp_p - k \| &= \arg \min_{p_p} \| M^T Mp_p - M^T k \| \\ &= \arg \min_{p_p} \| p_p - (M^T M)^{-1} M^T k \| \end{aligned}$$

As a result, we need only compute $(M^T M)^{-1} M^T k$ to recover parameter vector p_p , the unknown plane parameters, $p_p = \{b_p, c_p, d_p\}$. This formulation is performed iteratively from which the plane fit, parametrized as p_p , with the minimal error, ϵ , over N RANSAC iterations is selected within each sliding window. Empirically we use $N = 30$, for each window location within the vertical search (Figure 4) and a plane is identified when the resulting fitting error is below a given threshold, $\epsilon < \tau_{plane}$ (normalized for volume size, $\tau_{plane} = 7$, i.e. ± 7 mm from the plane). An example of a plane, detected within the CT volume shown in Figure 3, is shown in Figure 5. In this example we see two views (Figure 5 A / B) of a plane detected within the liquid density range voxels that remain after pre-processing (Section III-A). This plane (shown top-down Figure 5A) corresponds to the liquid surface of a bottle object within the volume (shown side-on in Figure 5B).

C. 2D Elliptical Fitting

Our second stage of shape fitting identifies ellipses which bound the possible liquid surfaces within the surface plane identified in the previous stage of planar fitting. This choice of an elliptical model for 2D fitting within the plane results from the aforementioned property of the morphological lucidity of the liquid to adapt to any given container. For example Figure 6 (right), a top view of two planar slices containing detected liquid surfaces, shows that despite the variance in the primary shape of given container (shown in blue in the Figure 6, right) an ellipsoid model represents a good generalized bounding model to circular, rectangular or indeed elliptical container types.

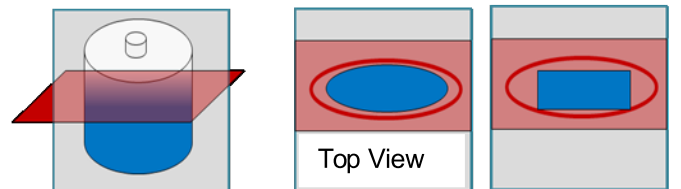


Figure 6. Illustration of the liquid property to adapt to its container

From the comprehensive review of geometric elliptical fitting in [14], we use a least squares technique that aims to minimize the overall square error term between the ellipse model and the corresponding data points. The general equation for a 2D ellipse, with radii r_{major} and r_{minor} at centered at position (h, k) with its major axis (corresponding to r_{major})

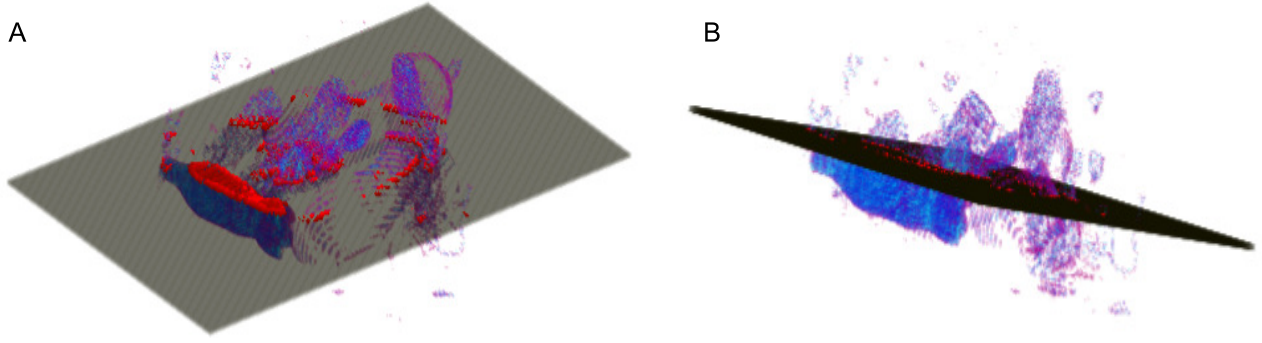


Figure 5. An 3D plane detected within the remaining liquid density range voxels of Figure 3

at angle θ to the x -axis is defined as follows:

$$\begin{aligned}
 f_{\text{ellipse}}(x, y) &= \frac{((x - h) \cos \theta + (y - k) \sin \theta)^2}{(r_{\text{major}}^2)} \\
 &+ \frac{((x - h) \sin \theta - (y - k) \cos \theta)^2}{(r_{\text{minor}}^2)} \\
 &= 1
 \end{aligned} \quad (6)$$

where we consider a 2D point (x, y) on an $x \leftrightarrow y$ plane (parametrized within plane identified III-B, separate from the axis definitions of Section III-B) as being inside the ellipse for $f_{\text{ellipse}}(x, y) \leq 1$ and outside the ellipse otherwise. Expansion of Eqn. 6 allows representation in implicit form as [14] such that a given elliptical curve is represented as parameter vector, $p_e = (a_e, b_e, c_e, d_e, e_e, f_e)'$, within the following:

$$\begin{aligned}
 F(p_e; (x, y)) &= a_e x^2 + b_e y^2 + c_e xy + d_e x + e_e y + f_e \\
 &= [x^2, y^2, xy, x, y, 1] \cdot p_e \\
 &= 0
 \end{aligned} \quad (7)$$

From which we formulate a least squares solution to Eqn. 7 which minimizes the squared error term of the algebraic distances, ϵ^2 , over the set of sample n points such that $\epsilon^2(p_e) = \sum_{i=0}^n F(p_e; (x_i, y_i))^2$. This is then minimized following [14] to determine the optimal least squares fit as $\arg_{p_e} \min(\epsilon^2(p_e))$.

Within our isolated 3D plane (Section III-B) elliptical fitting is iteratively applied to a sub-set of the remaining planar data points (after pre-processing, Section III-A) which correspond to a consistent edge-tracked contour within this plane (using [23]). Elliptical fitting is subsequently performed over this identified set of contour points following [14], resulting in a parametrized representation of each ellipse, p_e , from which we can recover the radii, angular offset and centre point, $\{r_{\text{major}}, r_{\text{minor}}, \theta, (h, k)\}$ (Eqn. 6).

Empirically we observe that over a large range of exemplar images, liquid containers do not vary significantly within the characteristic and ratio of the minimum and the maximum diameter elliptical fit. Hence we empirically filter the resulting set of ellipse instances by radii to contain only those with $\{6.25\text{mm} < r_{\text{minor}} < 75\text{mm}\}$ and $\{28.75\text{mm} < r_{\text{major}} < 250\text{mm}\}$ (based on the voxel sampling density in millimetres (mm), Section IV). This results in a number of identified ellipses within the plane over which we apply an

elliptical fill criterion to discriminate the true liquid surface ellipses, corresponding to a region filled with liquid range density values (Section III-A), from those fitted to coincident noise patterns. For each remaining data point, (x_i, y_i) (within the density range for liquids, isolated in Section III-A) we apply Eqn. 6 populated with the corresponding parameters, $\{r_{\text{major}}, r_{\text{minor}}, \theta, (h, k)\}$, for each ellipse identified within the plane to form a ‘‘point in ellipse’’ test. A fill ratio, η , is then calculated as the number of sample points inside a given ellipse against the total area of the fitted ellipse ($\pi r_{\text{minor}} r_{\text{major}}$) with reference to the voxel sampling density (in millimetres (mm), Section IV). Empirically, ellipses with a filling ratio $\eta \geq 0.85$ (85%) are retained.

The key steps within this process are illustrated by example in Figure 7. Here we see the original liquid density data points within a plane (Section III-B) that have been retained after pre-processing (Section III-A) in Figure 7A together with the subset corresponding to tracked contours (Figure 7B), the resulting ellipses recovered via fitting (Figure 7C) and those that are retained after radii and fill filtering is applied (Figure 7D, red). It is noted that this combination of pre-fit filtering based on contour connectedness and post-fitting filtering based on radii and fill ratio criteria eliminates all of the non-liquid ellipses within the example (Figure 7 A-D). Furthermore, it should be noted that the pre-filtering is highly inclusive in nature resulting in a significant number of liquid surface candidates as a result of ellipse fitting itself (Figure 7C). It is the later radii and fill ratio criteria that identifies the liquid surface within this plane despite the fact it does not correspond precisely to an elliptical shape (Figure 7D, red). This supports the case for the use of a generalized elliptical model in the identification of liquid container surface regions within 2D volume slice images.

The ellipse identified within Figure 7D can be back-projected for visualization within the original 2D plane identified in the 3D CT volume (Figure 8A, light blue) and additionally back to the 3D CT volume itself (Figure 8B, light blue). Within context, the visualization of the elliptical liquid surface within Figure 8B, is illustrative of the type of image overlay that could be used for operator alerting within a multi-stage baggage screening process incorporating 3D volume visualization of the 3D CT scan imagery.

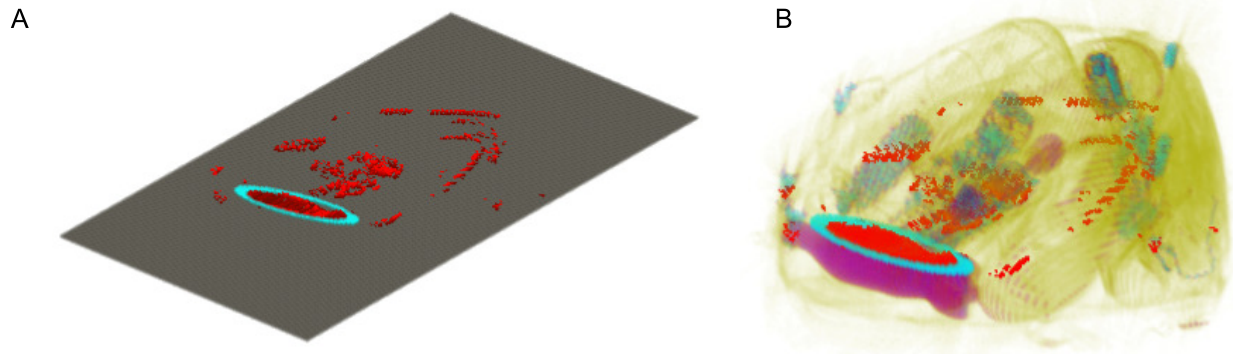


Figure 8. Identified ellipse corresponding to liquid surface within the plane (A) back-projected into the original CT volume image (B)

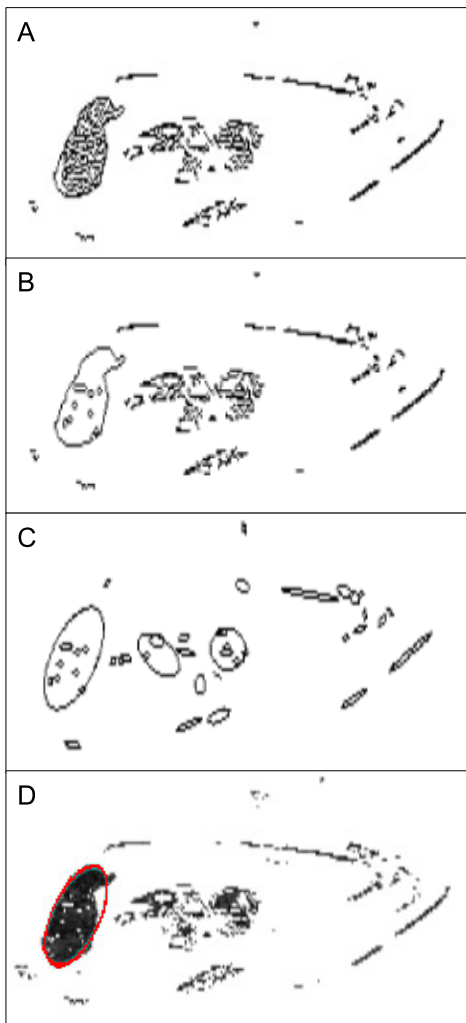


Figure 7. Original liquid density data points within the plane (A) with corresponding contours (B), resulting fitted ellipses (C) and those retained after radii and fill filtering (D, highlighted in red).

IV. RESULTS

Results are presented detailing the performance of 3D planar fitting (in isolation) and the combined use of 2D secondary elliptical fitting for liquid surface detection. These are presented using a set of volumes with an original voxel sampling of

$[1.6mm \times 1.6mm \times 5mm]$, subsequently re-sampled (using cubic spline interpolation) to form cubic voxels of uniform $2.5mm$ sampling in all axes [7]. All data was gathered using a CT-80 XL 3D baggage scanner manufactured by Reveal Imaging Technologies.

Our experimentation has been performed over a homogeneous composition of physical baggage prepared for a range of experimentation processes including recognized certification trials [9], [10], [7], [8], [11]. The test baggage items contain all manner of articles (clothes, shoes, electronics devices, liquids, books, weapons and other domestics travel items). In order to have a representative sample of common consumer liquid containers within the baggage we include a large variety of liquid types (water, soda, shampoo, hand gel, spray, milk, toothpaste, etc). The liquids items were filled at different levels (full, part filled, or almost empty) and also placed in the baggage in varying positions to allow us to evaluate the algorithm over a wide variety of baggage and liquid containers configuration/orientations with the knowledge that the scanning protocol (~ 30 seconds per bag scan) is sufficient to let any liquid reach a stable state (i.e. the surface of the liquid to be horizontal to the ground plane). This protocol follows current operational conditions for this scanner. Additionally a set of clear bags with no liquid containers present were also scanned to allow us to test for false positive detection.

Table I show the performance of the proposed technique over a set of 100 baggage items, of which 15 items did not contain any liquid containers (clear bags). These were constructed as described with one or more liquid containers within the non-clear baggage items. Results are shown (by percentage) in terms of True Positive (TP), True Negative (TN), False Positive (FP) and False Negative (FN) detections for both initial 3D planar fitting (result set A: to detect a plane containing liquid surface(s) is within the volume) and with additional subsequent 2D elliptical fitting (to localize liquid container surfaces within that identified plane). For clarity:

- TP: a liquid surface is present within the volume and is correctly detected as either a plane within the volume (Table I, result set A) or is subsequently localized to the correct liquid container within that plane (Table I, result set B).
- TN: the volume contains no liquid surfaces and none are detected as plane within the volume (Table I, result set

Result Set	True Positive (TP)	True Negative (TN)	False Positive (FP)	False Negative (FN)	Accuracy	Precision	Recall	TNR
A: 3D Planar Fitting (only)	98%	100%	0%	2%	0.99	1.00	0.98	1.000
B: 3D Planar Fitting + 2D Elliptical Fitting	85%	(100%)	12%	3%	1.00	0.88	0.97	0.999

Table I
RESULTS OF 3D PLANAR FITTING AND 2D ELLIPTICAL FITTING FOR LIQUID SURFACE DETECTION

A).

- FP: the volume contains no liquid surfaces but one or more are detected as plane within the volume (Table I, result set A) or an ellipse is detected that corresponds to a non-liquid surface item within a previously identified plane (i.e. incorrect localization; Table I, result set B).
- FN: a liquid surface is present within the volume and is either not detected as either a plane within the volume (Table I, result set A) or is subsequently incorrectly localized to the correct liquid container within that plane (Table I, result set B).

As we can see from Table I (result set A), our approach correctly detects the presence of a liquid surface within the CT volume in 98% of cases (TP) and presents no FP detections (via 3D planar fitting, Section III-B). FN are marginal (2%) and corresponds to very small or dispersed (complex geometry) liquid containers. From this set of detected liquid planes, our second stage of detection (via 2D elliptical fitting, Section III-C) correctly localizes the liquid surface within that plane in 85% of cases (TP), completely misses the surface location in 3% of cases (FN) and incorrectly localizes it within the plane in 12% of cases (FP) (Table I, result set B). Both approaches perform favourably with respect to the conventional statistical measures of accuracy, precision, recall and true negative rate (TNR) which are defined as follows:-

$$Accuracy = \frac{tp + tn}{tp + fp + tn + fn} \quad (8)$$

$$Precision = \frac{tp}{tp + fp} \quad (9)$$

$$Recall = \frac{tp}{tp + fn} \quad (10)$$

$$TrueNegativeRate (TNR) = \frac{tn}{tn + fp} \quad (11)$$

Overall we see high accuracy, precision and recall supported by a high true negative rate that is indicative of the low false alarm (i.e. FP) performance achieved (Table I).

Examples of missed liquid surfaces (FN) are shown in Figure 9 where we see both examples of a failure within the initial detection of the plane within the volume (Figure 9, left) and also where ellipse localization within the plane has failed (Figure 9, middle / right). Conversely, two FP liquid surface ellipses are shown in Figure 10 where we see the coincidental alignment of noise forming a consistent ellipse FP (Figure 10 left) and (Figure 10 right, leftmost ellipse instance). These form part of the 12% FP that do not necessarily indicate a

poor result overall as, even if the shape of the liquid surface is not highlighted with a fitted ellipse, the liquid surface still appears on detected 3D plane. A range of successful liquid surface detection (TP) are shown in Figure 11 where we see successful localization of the liquid surface within the plane extracted from the volume (Figure 11, left in red) and re-projection back into the volume (Figure 11, right in light blue). Figure 12 shows a wider range of TP detections, as ellipses within the detected 3D plane (Figure 12, red) and also examples where despite initial detection of the plane within the volume, elliptical localization of the liquid surface within the plane has failed (FN, Figure 12, blue).

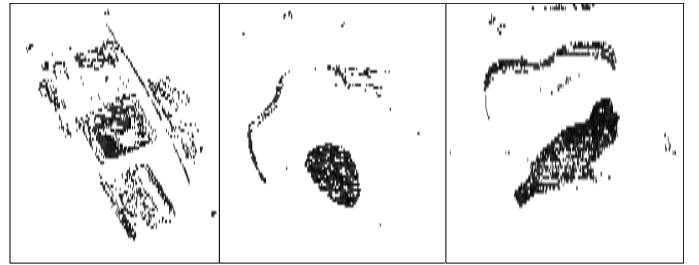


Figure 9. Three examples of false negatives where a liquid surface was either not detected as a plane within the volume (left) or as an ellipse within the plane (middle and right).

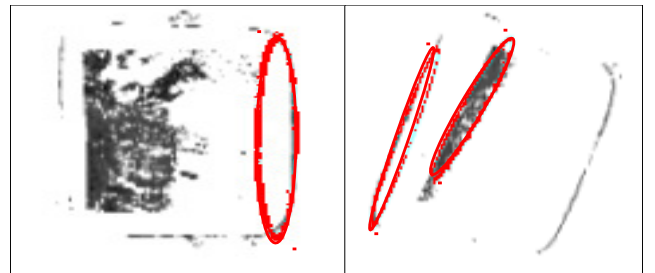


Figure 10. Two examples of false positives liquid surface detection as an ellipse within the plane.

V. CONCLUSIONS

We have developed an approach for automatic detection of liquid surfaces within 3D CT baggage imagery which is based on a two stage process of 3D planar fitting within the volume and subsequent 2D elliptical fitting for localization within the identified plane. This gives highly satisfactory results with 98% of planes containing liquid surfaces detected within the volume and subsequently 85% of liquid surfaces subsequently localized correctly within the plane. This detection of liquid

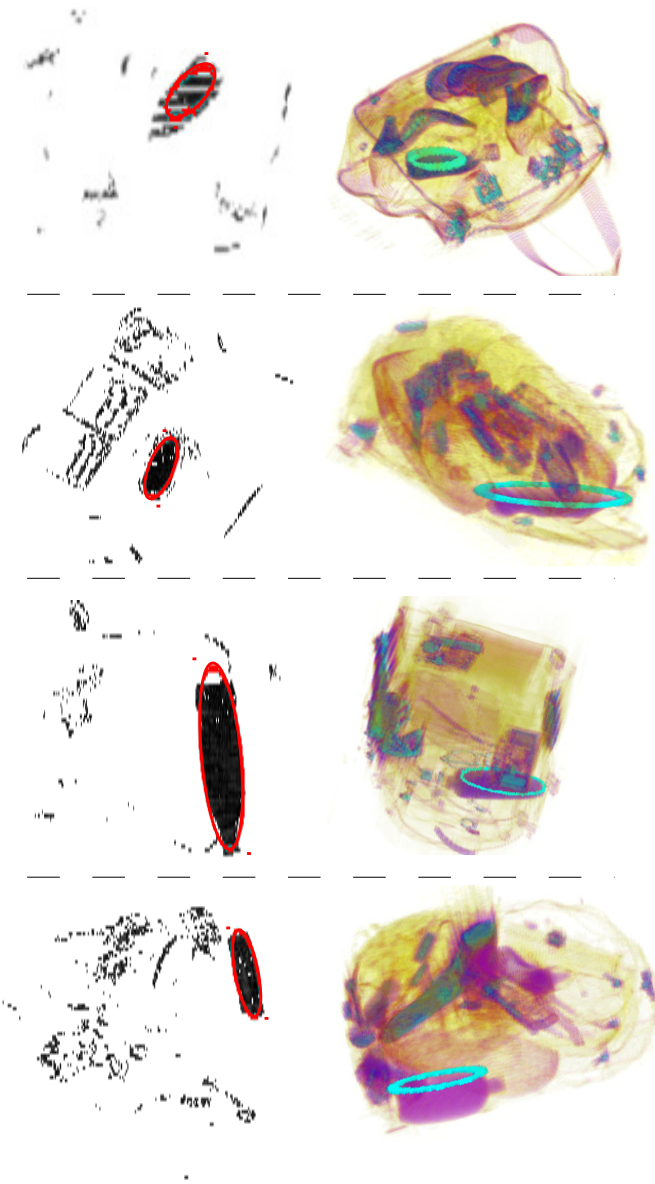


Figure 11. Examples of true positive detection of liquid planes both as a ellipse within the plane (right, red) and back-projected into the original CT baggage volume (left, light blue).

present and its localization within the 3D CT volume is achieved based on robust geometrical fitting, and 3D shape understanding, without a dependence on exemplar training data such as other contemporary approaches within the domain [9], [10], [7], [8], [11], [20], [2]. Furthermore the 3D fitting approach outlined extends prior work in the field [21] in terms of stability to noise and surface variation with the addition of second stage elliptical fitting. Overall the work has shown that geometric approach to liquid detection without reference to an explicit set of training data can provide a valuable solution to liquid detection and voxelization within 3D CT baggage imagery. Future work will examine the use of combined planar and elliptic fitting in addition to integration with further materials based discrimination techniques [2].

Acknowledgments: This work was funded under the Innovative Research Call in Explosives and Weapons Detection

(2010), sponsored by UK Home Office Scientific Development Branch (HOSDB), Department for Transport, Centre Protection of National Infrastructure (CNPI) and the Metropolitan Police Service.

REFERENCES

- [1] G. Flitton, A. Mouton, and T. P. Breckon, "Object classification in 3D baggage security computed tomography imagery using visual code-books," *Pattern Recognition*, vol. 48, pp. 2489–2499, Aug. 2015.
- [2] A. Mouton and T. P. Breckon, "Materials-based 3D segmentation of unknown objects from dual-energy computed tomography imagery in baggage security screening," *Pattern Recognition*, vol. 48, pp. 1961–1978, June 2015.
- [3] N. E. L. Shanks and A. L. W. Bradley, *Handbook of Checked Baggage Screening: Advanced Airport Security Operation*. Wiley, isbn: 978- ed., 2004.
- [4] S. Singh and M. Singh, "Explosives detection systems (EDS) for aviation security," *Signal Processing*, vol. 83, no. 1, pp. 31–55, 2003.
- [5] T. R. Johnson, *Medical radiology/diagnostic imaging: dual energy CT in clinical practice*. Springer, 2011.
- [6] B. R. Abidi, Y. Zheng, A. V. Gribok, and M. A. Abidi, "Improving weapon detection in single energy X-ray images through pseudocoloring," *IEEE Transactions on Systems, Man, and Cybernetics, Part C: Applications and Reviews*, vol. 36, no. 6, pp. 784–796, 2006.
- [7] G. T. Flitton, T. P. Breckon, and N. Megherbi, "Object Recognition using 3D SIFT in Complex CT Volumes," in *Proc. British Machine Vision Conference*, pp. 11.1–12, Sept. 2010.
- [8] G. T. Flitton, T. P. Breckon, and N. Megherbi, "A 3D Extension to Cortex Like Mechanisms for 3D Object Class Recognition," in *Proc. International Conference on Computer Vision and Pattern Recognition*, pp. 3634–3641, IEEE, June 2012.
- [9] N. Megherbi, G. T. Flitton, and T. P. Breckon, "A Classifier based Approach for the Detection of Potential Threats in CT based Baggage Screening," in *Proc. International Conference on Image Processing*, pp. 1833–1836, Sept. 2010.
- [10] N. Megherbi, J. Han, T. P. Breckon, and G. T. Flitton, "A comparison of classification approaches for threat detection in CT based baggage screening," in *2012 19th IEEE International Conference on Image Processing*, pp. 3109–3112, IEEE, Sept. 2012.
- [11] G. T. Flitton, T. P. Breckon, and N. Megherbi, "A Comparison of 3D Interest Point Descriptors with Application to Airport Baggage Object Detection in Complex CT Imagery," *Pattern Recognition*, 2013.
- [12] F. Tarsha-Kurdi, T. Landes, and P. Grussenmeyer, "Hough-Transform and Extended RANSAC Algorithms for Automatic Detection of 3D Building Roof Planes from Lidar Data," 2007.
- [13] V. Pratt, "Direct least-squares fitting of algebraic surfaces," in *Proceedings of the 14th annual conference on Computer graphics and interactive techniques - SIGGRAPH '87*, vol. 21, (New York, New York, USA), pp. 145–152, ACM Press, Aug. 1987.
- [14] A. Fitzgibbon, M. Pilu, and R. Fisher, "Direct least square fitting of ellipses," *IEEE Transactions on Pattern Analysis and Machine Intelligence*, vol. 21, pp. 476–480, May 1999.
- [15] L. Eger, P. Ishwar, W. Karl, and H. Pien, "Classification-aware dimensionality reduction methods for explosives detection using multi-energy X-ray computed tomography," in *SPIE Electronic Imaging*, pp. 78730Q–78730Q, International Society for Optics and Photonics, 2011.
- [16] A. Mouton, N. Megherbi, T. Breckon, K. Van Slambrouck, and J. Nuyts, "A distance driven method for metal artefact reduction in computed tomography," in *Proceedings IEEE International Conference on Image Processing*, pp. 2334–2338, 2013.
- [17] A. Mouton, N. Megherbi, G. T. Flitton, and T. P. Breckon, "A Novel Intensity Limiting Approach to Metal Artefact Reduction in 3D [CT] Baggage Imagery," in *Proc. International Conference on Image Processing*, IEEE, Sept. 2012.
- [18] A. Mouton, N. Megherbi, K. van Slambrouck, J. Nuyts, and T. Breckon, "An experimental survey of metal artefact reduction in computed tomography," *Journal of X-Ray Science and Technology*, vol. 21, no. 2, pp. 193–226, 2013.
- [19] W. Bi, Z. Chen, L. Zhang, and Y. Xing, "A volumetric object detection framework with dual-energy CT," in *IEEE Nuclear Science Symposium Conference Record*, 2008., pp. 1289–1291, Oct. 2008.
- [20] A. Mouton, T. P. Breckon, G. T. Flitton, and N. Megherbi, "3D object classification in baggage computed tomography imagery using randomised clustering forests," in *2014 IEEE International Conference on Image Processing (ICIP)*, pp. 5202–5206, IEEE, Oct. 2014.

- [21] W. Bi, Z. Chen, L. Zhang, and Y. Xing, "Fast detection of 3D planes by a single slice detector helical CT," in *Proceedings of the IEEE Nuclear Science Symposium Conference Record*, pp. 954–955, 2009.
- [22] M. Fischler and R. Bolles, "Random Sample Consensus: A Paradigm for Model Fitting With Applications to Image Analysis and Automated Cartography," *Communications of the ACM*, vol. 24, no. 6, pp. 381–395, 1981.
- [23] D. H. DOUGLAS and T. K. PEUCKER, "ALGORITHMS FOR THE REDUCTION OF THE NUMBER OF POINTS REQUIRED TO REPRESENT A DIGITIZED LINE OR ITS CARICATURE," *Cartographica: The International Journal for Geographic Information and Geovisualization*, vol. 10, pp. 112–122, Oct. 1973.

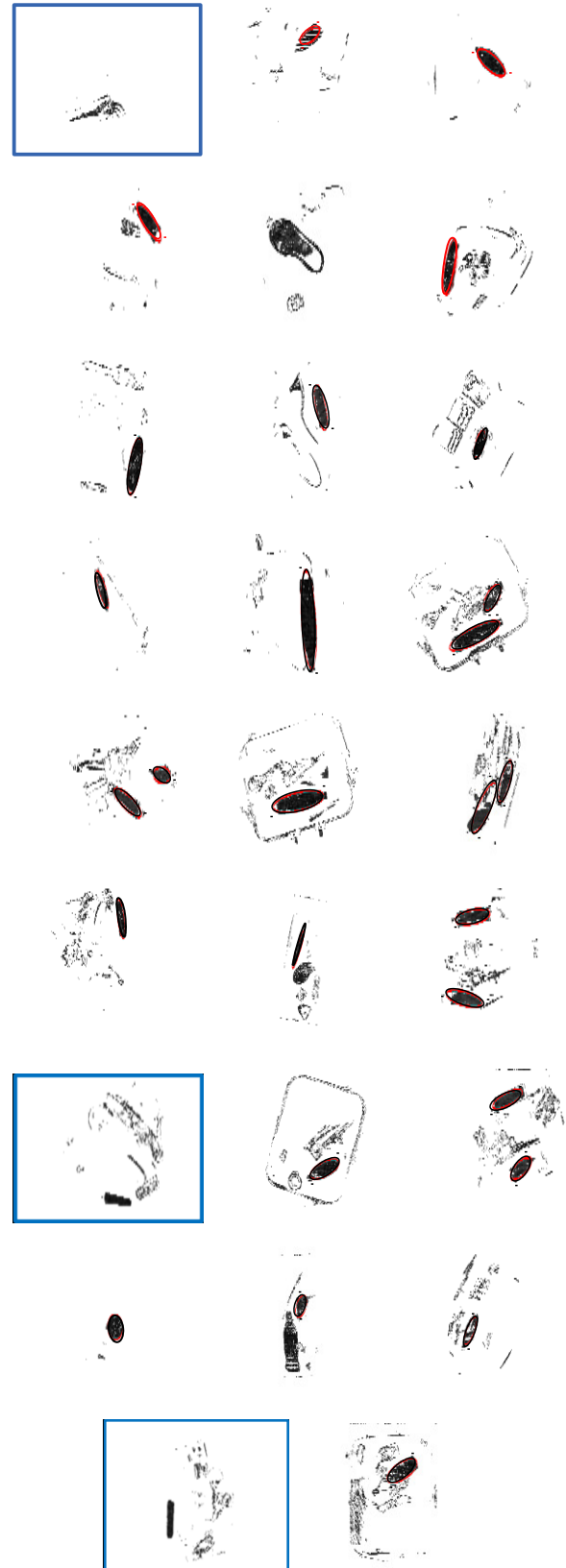


Figure 12. Examples of true positive detection of liquid planes as an ellipse within the plane (red) and false negative examples of failed ellipse localization within a detected liquid containing plane (blue).